

WASP-20b and WASP-28b: a hot Saturn and a hot Jupiter in near-aligned orbits around solar-type stars[★]

D. R. Anderson¹, A. Collier Cameron², C. Hellier¹, M. Lendl³, T. A. Lister⁴, P. F. L. Maxted¹, D. Queloz^{3,5}, B. Smalley¹, A. M. Smith^{1,6}, A. H. M. J. Triaud^{3,7}, D. J. A. Brown^{8,9}, M. Gillon¹⁰, M. Neveu-VanMalle³, F. Pepe³, D. Pollacco⁸, D. Ségransan³, S. Udry³, R. G. West⁸, and P. J. Wheatley⁸

¹ Astrophysics Group, Keele University, Staffordshire ST5 5BG, UK
e-mail: d.r.anderson@keele.ac.uk

² SUPA, School of Physics and Astronomy, University of St. Andrews, North Haugh, Fife KY16 9SS, UK

³ Observatoire de Genève, Université de Genève, 51 Chemin des Maillettes, 1290 Sauverny, Switzerland

⁴ Las Cumbres Observatory Global Telescope Network, 6740 Cortona Dr. Suite 102, Goleta, CA 93117, USA

⁵ Cavendish Laboratory, J J Thomson Avenue, Cambridge, CB3 0HE, UK

⁶ N. Copernicus Astronomical Centre, Polish Academy of Sciences, Bartycza 18, 00-716, Warsaw, Poland

⁷ Department of Physics, and Kavli Institute for Astrophysics and Space Research, MIT, Cambridge, MA 02139, USA

⁸ Department of Physics, University of Warwick, Coventry CV4 7AL, UK

⁹ Astrophysics Research Centre, School of Mathematics & Physics, Queen's University, University Road, Belfast BT7 1NN

¹⁰ Institut d'Astrophysique et de Géophysique, Université de Liège, Allée du 6 Août, 17, Bat. B5C, Liège 1, Belgium

Received February 6, 2014 / accepted Month DD, YEAR

ABSTRACT

We report the discovery of the planets WASP-20b and WASP-28b along with measurements of their sky-projected orbital obliquities. WASP-20b is an inflated, Saturn-mass planet ($0.31 M_{\text{Jup}}$; $1.46 R_{\text{Jup}}$) in a 4.9-day, near-aligned ($\lambda = 8.1 \pm 3.6^\circ$) orbit around CD-24 102 ($V=10.7$; F9). WASP-28b is an inflated, Jupiter-mass planet ($0.91 M_{\text{Jup}}$; $1.21 R_{\text{Jup}}$) in a 3.4-day, near-aligned ($\lambda = 8 \pm 18^\circ$) orbit around a $V=12$, F8 star. As intermediate-mass planets in short orbits around aged, cool stars (7^{+2}_{-1} Gyr for WASP-20 and 5^{+3}_{-2} Gyr for WASP-28; both with $T_{\text{eff}} < 6250$ K), their orbital alignment is consistent with the hypothesis that close-in giant planets are scattered into eccentric orbits with random alignments, which are then circularised and aligned with their stars' spins via tidal dissipation.

Key words. planetary systems – stars: individual: WASP-20 – stars: individual: WASP-28

1. Introduction

Planets that transit relatively bright host stars ($V < 13$) are providing a rich source of information for the nascent field of exoplanetology. To date, the main discoverers of these systems are the ground-based transit surveys HATNet and SuperWASP and the space mission Kepler (Bakos et al. 2004; Pollacco et al. 2006; Borucki et al. 2010).

One parameter that, uniquely, we can determine for transiting planets is obliquity (Ψ), the angle between a star's rotation axis and a planet's orbital axis. We do this by taking spectra of a star during transit: as the planet obscures a portion of the rotating star it causes a distortion of the observed stellar line profile, which manifests as an anomalous radial-velocity (RV) signature known as the Rossiter-McLaughlin (RM) effect (Rossiter 1924; McLaughlin 1924). The shape of the RM effect is sensitive to the path a planet takes across the disc of a star relative to the stellar spin axis. If we have a constraint on the inclination of the stellar spin axis relative to the sky plane (I_*), then we can de-

termine the true obliquity (Ψ), otherwise we can only determine the sky-projected obliquity (λ). The two are related by:

$$\cos \Psi = \cos I_* \cos i_p + \sin I_* \sin i_p \cos \lambda$$

where i_p is the inclination of the orbital axis to the sky plane.

The obliquity of a short-period, giant planet may be indicative of the manner in which it arrived in its current orbit from farther out, where it presumably formed. As the angular momenta of a star and its planet-forming disc both derive from that of their parent molecular cloud, stellar spin and planetary orbital axes are expected to be, at least initially, aligned. Migration via tidal interaction with the gas disc is expected to preserve initial spin-orbit alignment (Lin et al. 1996; Marzari & Nelson 2009), but almost half (33 of 74) of the orbits so far measured are misaligned and approximately 10 of those are retrograde.¹

These results are consistent with the hypothesis that some or all close-in giant planets arrive in their orbits by planet-planet and/or star-planet scattering, which can drive planets into eccentric, misaligned orbits, and tidal friction, which circularises, shortens and aligns orbits (see the following empirical-based papers: Triaud et al. 2010; Winn et al. 2010; Naoz et al. 2011; Albrecht et al. 2012; also see the following model-based papers: Fabrycky & Tremaine 2007; Nagasawa et al. 2008; Matsumura et al. 2010; Naoz et al. 2011).

[★] Based on observations made with: the WASP-South (South Africa) and SuperWASP-North (La Palma) photometric survey instruments; the C2 and EulerCam cameras and the CORALIE spectrograph, all mounted on the 1.2-m Euler-Swiss telescope (La Silla); the HARPS spectrograph on the ESO 3.6-m telescope (La Silla) under programs 072.C-0488, 082.C-0608, 084.C-0185 and 085.C-0393; and LCOGT's Faulkes Telescope North (Maui) and Faulkes Telescope South (Siding Spring).

¹ René Heller maintains a list of measurements and references at http://www.physics.mcmaster.ca/~rheller/content/main_HRM.html

Systems with short tidal timescales (those with short scaled orbital major semi-axes, a/R_* , and high planet-to-star mass ratios) tend to be aligned (Albrecht et al. 2012 and references therein). A broad range of obliquities is observed for stars with $T_{\text{eff}} > 6250$ K, for which tidal realignment processes may be inefficient due to the absence of a substantial convective envelope (Winn et al. 2010; Schlaufman 2010). Limiting focus to stars more massive than $1.2 M_{\odot}$, for which age determinations are more reliable, Triaud (2011) noted that systems older than 2.5 Gyr tend to be aligned; this could be indicative of the time required for orbital alignment or of the timescale over which hotter stars develop a substantial convective envelope as they evolve.

A major hurdle to overcome for any hypothesis involving realignment is tidal dissipation seems to cause both orbital decay and realignment on similar timescales (Barker & Ogilvie 2009). Alternative hypotheses suggest that misalignments arise via re-orientations of either the disc or the stellar spin and that migration then proceeds via planet-disc interactions (e.g. Bate et al. 2010; Lai et al. 2011; Rogers et al. 2012). However, observations of debris discs well aligned with their stellar equators suggest that tilting of the star or the disc rarely occurs (Greaves et al. 2014).

Here we present the discovery and obliquity determinations of the two new transiting planets WASP-20b (CD-24 102) and WASP-28b (2MASS J23342787–0134482), and interpret the results under the hypothesis of migration via scattering and tidal dissipation.

2. Observations

We provide a summary of observations in Table 1. The WASP (Wide Angle Search for Planets) photometric survey (Pollacco et al. 2006) monitors bright stars ($V = 9.5\text{--}13.5$) using two eight-camera arrays, each with a field of view of 450 deg^2 . Each array observes up to eight pointings per night with a cadence of 5–10 min, and each pointing is followed for around five months per season. The WASP-South station (Hellier et al. 2011) is hosted by the South African Astronomical Observatory and the SuperWASP-North station (Faedi et al. 2011) is hosted by the Isaac Newton Group at the Observatorio del Roque de Los Muchachos on La Palma. The WASP data were processed and searched for transit signals as described in Collier Cameron et al. (2006) and the candidate selection process was performed as described in Collier Cameron et al. (2007). We observed periodic dimmings in the WASP lightcurves of WASP-20 and WASP-28 with periods of 4.8996 d and 3.4088 d, respectively (see the top panels of Figures 1 and 2). We searched the WASP lightcurves for modulation as could be caused by magnetic activity and stellar rotation (Maxted et al. 2011). We did not detect any significant, repeated signals and we find that any modulation must be below the 2-mmag level.

We obtained 56 spectra of WASP-20 and 26 spectra of WASP-28 with the CORALIE spectrograph mounted on the Euler-Swiss 1.2-m telescope (Baranne et al. 1996; Queloz et al. 2000). We obtained a further 63 spectra of WASP-20 with the HARPS spectrograph mounted on the 3.6-m ESO telescope (Mayor et al. 2003), including a sequence of 43 spectra taken through the transit of the night of 2009 October 22. We obtained a further 33 spectra of WASP-28 with HARPS, including 30 spectra taken through the transit of the night of 2010 August 17. Radial-velocity (RV) measurements were computed by weighted cross-correlation (Baranne et al. 1996; Pepe et al. 2005) with a numerical G2-spectral template (Table 2). We de-

Table 2. Radial-velocity measurements

Star	Spect.	BJD(UTC) –2450000 (day)	RV (km s^{-1})	σ_{RV} (km s^{-1})	BS (km s^{-1})
W-20	COR	4655.88265	1.3411	0.0074	0.0613
W-20	COR	4658.86065	1.2969	0.0103	0.0490
...					
W-28	HAR	5428.71664	24.2674	0.0098	0.0021
W-28	HAR	5428.86297	24.3180	0.0094	0.0145

The uncertainties are the formal errors (i.e. with no added jitter).

The uncertainties on the bisector spans (BS) are $2\sigma_{\text{RV}}$.

This table is available in its entirety via the CDS.

Table 3. Follow-up photometry

Set	Star	Tel.	BJD(UTC) –2450000 (day)	Flux, F	σ_F
1	W-20	FTN	4765.04209	0.99958	0.00179
1	W-20	FTN	4765.04283	1.00022	0.00163
...					
7	W-28	Euler	5443.88762	0.9971	0.0027
7	W-28	Euler	5443.88852	1.0006	0.0027

The flux values are differential and normalised to the out-of-transit levels.

The uncertainties are the formal errors (i.e. they have not been rescaled).

This table is available in its entirety via the CDS.

tected RV variations with periods similar to those found from the WASP photometry and with semi-amplitudes consistent with planetary-mass companions. We plot the RVs, phased on the transit ephemerides, in the third panel of Figures 1 and 2 and we highlight the RM effects in Figure 3

For each star, we tested the hypothesis that the RV variations are due to spectral-line distortions caused by a blended eclipsing binary or starspots by performing a line-bisector analysis of the cross-correlation functions (Queloz et al. 2001). The lack of any significant correlation between bisector span and RV supports our conclusion that the periodic dimming and RV variation of each system are caused by a transiting planet (Figure 4). This is further supported by our observation of the RM effect of each system: the $v \sin I_*$ values from our fits to the RM effects are consistent with the values we obtain from spectral line broadening (see Sections 3 and 4).

We performed follow-up transit observations to refine the systems' parameters using the 1.2-m Swiss Euler telescope (Lendl et al. 2012), and LCOGT's 2.0-m Faulkes Telescopes North and South (Brown et al. 2013). Some transit lightcurves were affected by technical problems or poor weather, as indicated in Table 1.

Table 1. Summary of observations

Facility	Date	N_{obs}	T_{exp} (s)	Filter	Issue
WASP-20:					
WASP-South	2006 May–2007 Nov	9 600	30	Broad (400–700 nm)	—
Euler/CORALIE	2008 Jul–2013 Oct	56	1800	Spectroscopy	—
ESO-3.6m/HARPS	2008 Aug–2011 Sep	20	600–1800	Spectroscopy	—
FTS/Spectral	2008 Oct 25	151	40	z'	autoguider
ESO-3.6m/HARPS	2009 Oct 22	43	300–400/1200	Spectroscopy	—
FTN/Merope	2011 Aug 20	70	70	z'	rotator
Euler/EulerCam	2011 Aug 29	237	20	Gunn- r	cloud
Euler/EulerCam	2011 Sep 03	156	70	Gunn- r	—
Euler/EulerCam	2011 Sep 08	201	30	Gunn- r	—
WASP-28					
WASP-South	2008 Jun–2009 Nov	10 100	30	Broad (400–700 nm)	—
SuperWASP-North	2008 Aug–2010 Sep	6 600	30	Broad (400–700 nm)	—
Euler/CORALIE	2009 Jun–2012 Dec	26	1800	Spectroscopy	—
FTN/Merope	2009 Oct 21	227	40	z'	unknown
ESO-3.6m/HARPS	2010 Aug 17–19	33	600/1200	Spectroscopy	—
Euler/C2	2010 Sep 03	217	25	Gunn- r	—

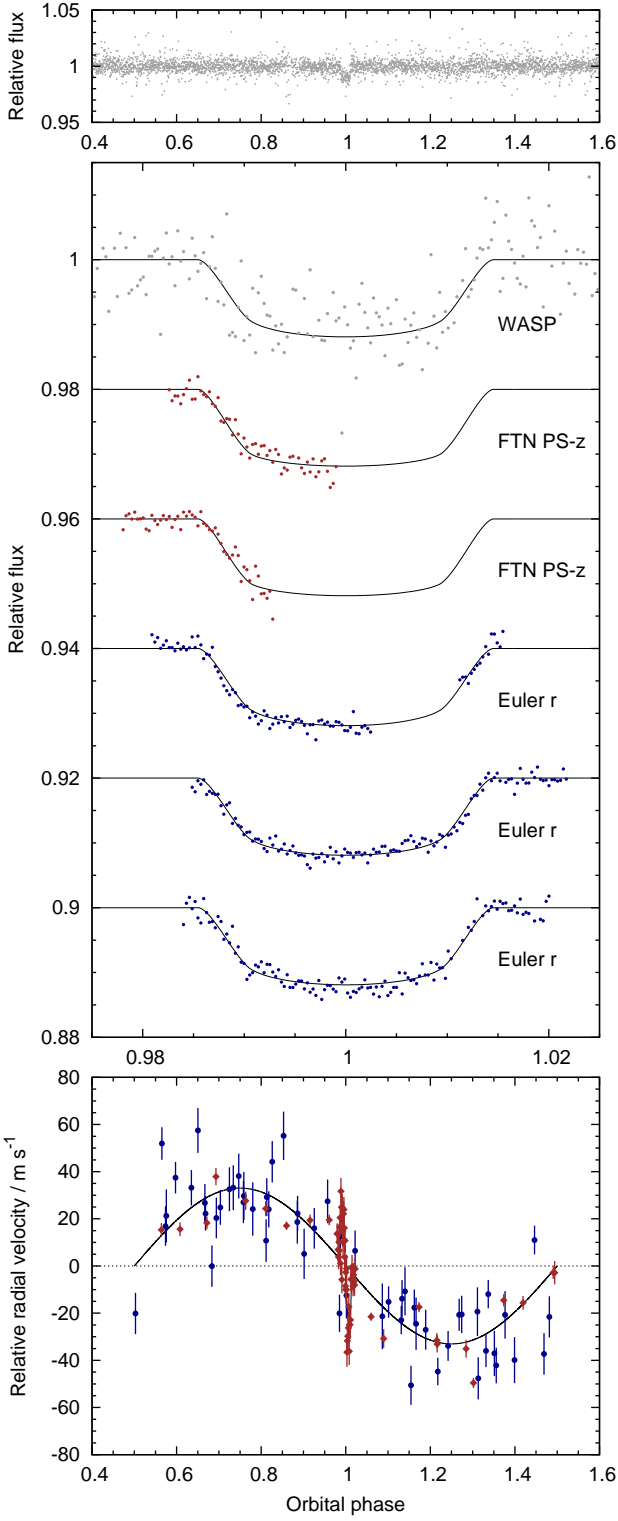


Fig. 1. WASP-20b discovery data. *Top panel:* WASP lightcurve folded on the transit ephemeris. *Middle panel:* Transit lightcurves from facilities as labelled, offset for clarity and binned with a bin width of two minutes. The best-fitting transit model is superimposed. *Bottom panel:* The radial velocities (CORALIE in blue, HARPS in brown) with the best-fitting circular Keplerian orbit model and the RM effect model.

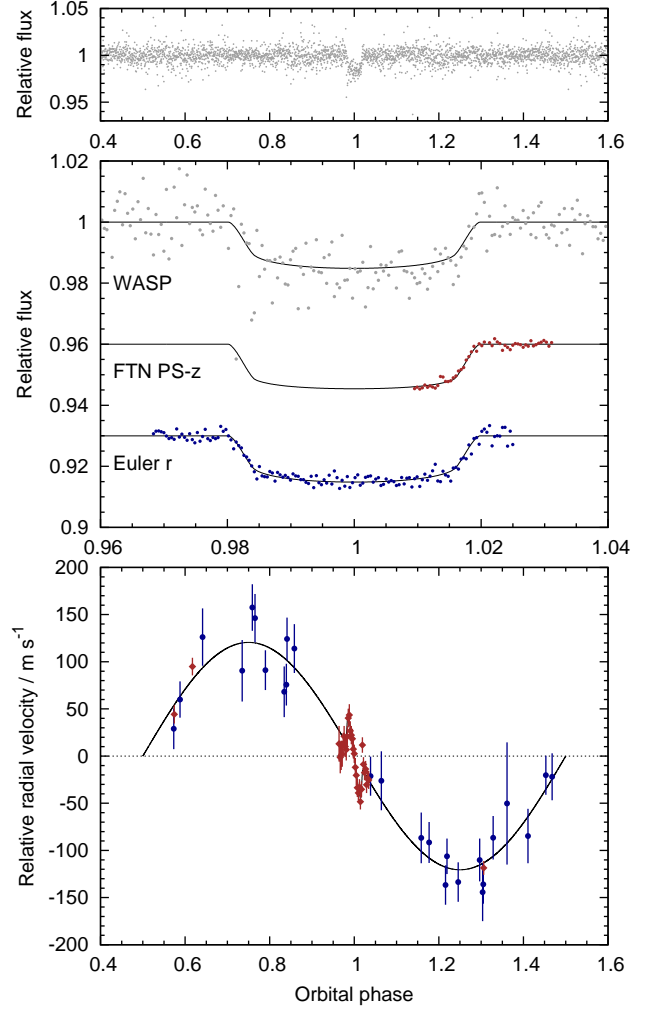


Fig. 2. WASP-28b discovery data. Caption as for Figure 1.

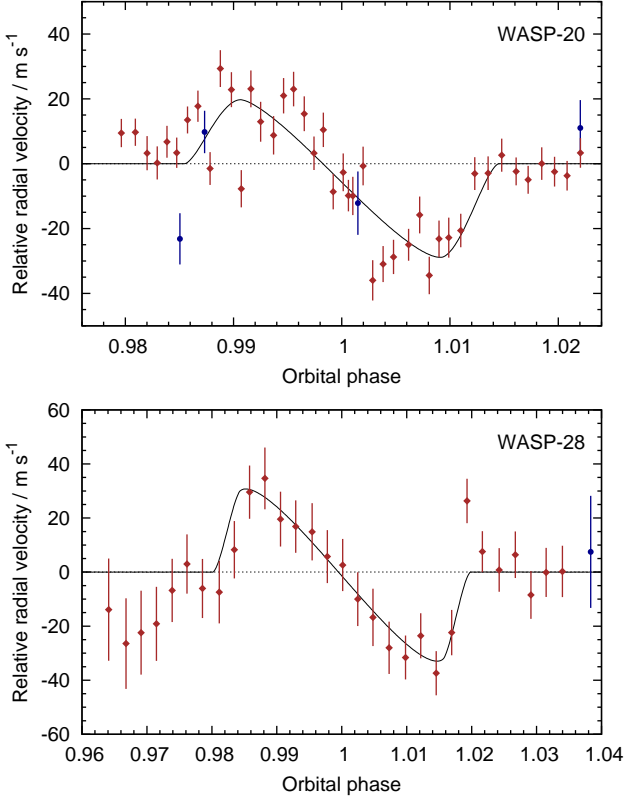


Fig. 3. The Rossiter-McLaughlin effects, or spectroscopic transits, of WASP-20b and WASP-28b. The CORALIE RVs are shown in blue and the HARPS RVs are shown in brown; the Keplerian orbits have been subtracted. For each planet, the observed apparent redshift, followed by an apparent blueshift of similar amplitude, indicate the orbit to be prograde and, probably, aligned with the stellar rotation. The alignment of the orbit of WASP-28b is less certain due to its low impact parameter. The lower precision of the earlier WASP-28 RVs resulted because the sequence started at an airmass of 1.7.

3. Stellar parameters from spectra

The 9 individual HARPS spectra from 2008 of WASP-20 were co-added and a total of 18 individual CORALIE spectra were co-added to produce one spectrum per star with typical S/N of 150:1 (WASP-20) and 70:1 (WASP-28). The standard pipeline reduction products were used in the analysis.

The analysis was performed using the methods given in Gillon et al. (2009). The H_α line was used to determine the effective temperature (T_{eff}), while the Na I D and Mg I b lines were used as surface gravity ($\log g_*$) diagnostics. The parameters obtained from the analysis are listed in Table 4. The elemental abundances were determined from equivalent width measurements of several clean and unblended lines. A value for microturbulence (ξ_t) was determined from Fe I using Magain’s (1984) method. The quoted error estimates include that given by the uncertainties in T_{eff} , $\log g_*$ and ξ_t , as well as the scatter due to measurement and atomic data uncertainties.

We assumed values for macroturbulence (v_{mac}) of 4.5 ± 0.3 km s $^{-1}$ and 4.7 ± 0.3 km s $^{-1}$ for WASP-20 and WASP-28, respectively. These were based on the tabulation by Gray (2008) and the instrumental FWHMs of 0.065 Å (HARPS) and 0.11 ± 0.01 Å (CORALIE), as determined from the telluric lines around 6300 Å. We determined the projected stellar rotation velocity

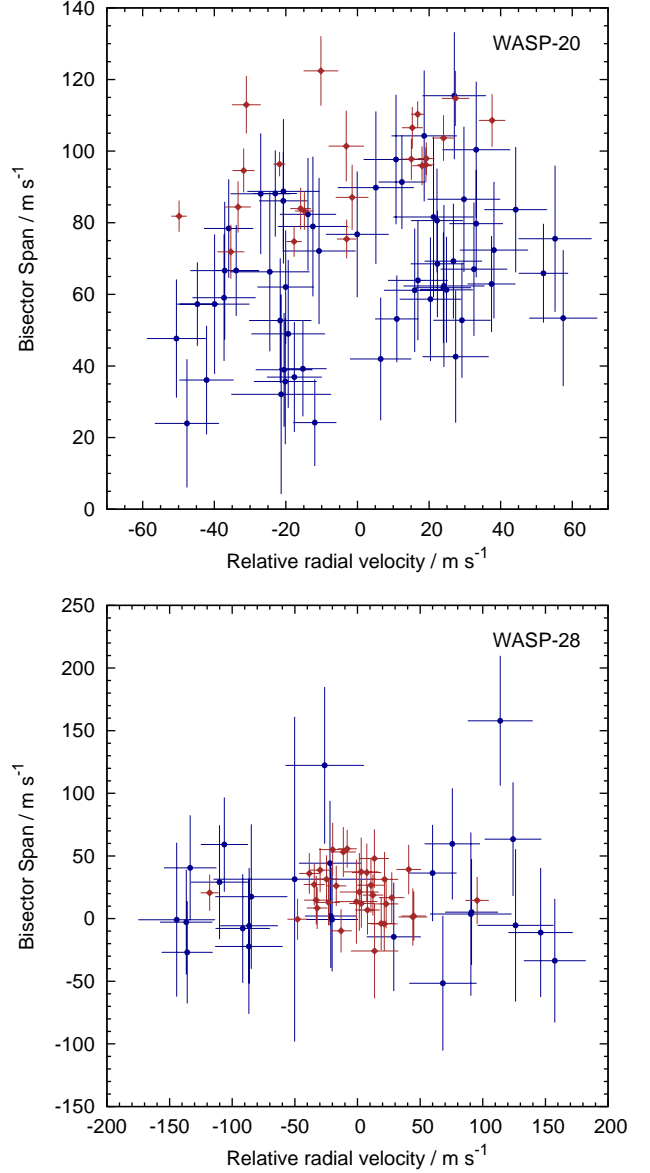


Fig. 4. The lack of any significant correlation between bisector span and radial velocity excludes transit mimics and supports our conclusion that each system contains a transiting planet.

($v \sin I_*$) by fitting the profiles of several unblended Fe I lines. We determined the $v \sin I_*$ of WASP-20 from the 62 HARPS spectra obtained up 2010 and the $v \sin I_*$ of WASP-28 from all 33 available HARPS spectra.

4. System parameters from the RV and transit data

We determined the parameters of each system from a simultaneous fit to the lightcurve and radial-velocity data. The fit was performed using the current version of the Markov-chain Monte Carlo (MCMC) code described by Collier Cameron et al. (2007) and Pollacco et al. (2008).

The transit lightcurves are modelled using the formulation of Mandel & Agol (2002) with the assumption that the planet is much smaller than the star. Limb-darkening was accounted for using a four-coefficient, nonlinear limb-darkening model, using coefficients appropriate to the passbands from the tabulations of Claret (2000, 2004). The coefficients are interpolated once using

Table 4. Stellar parameters from the spectra

Parameter	WASP-20	WASP-28
Star	CD-24 102	2MASS J23342787-0134482
Constellation	Cetus	Pisces
R.A. (J2000)	00 ^h 20 ^m 38 ^s .53	23 ^h 34 ^m 27 ^s .87
Dec. (J2000)	-23°56′08″.6	-01°34′48″.2
<i>B</i>	11.17	12.50
<i>V</i>	10.68	12.03
<i>J</i>	9.70	11.08
<i>H</i>	9.42	10.76
<i>K</i>	9.39	10.73
T_{eff}	6000 ± 100 K	6100 ± 150 K
log g_*	4.40 ± 0.15	4.5 ± 0.2
ξ_t	1.2 ± 0.1 km s ⁻¹	1.2 ± 0.1 km s ⁻¹
$v \sin I_*$	3.5 ± 0.5 km s ⁻¹	3.1 ± 0.6 km s ⁻¹
[Fe/H]	-0.01 ± 0.06	-0.29 ± 0.10
[Si/H]	+0.03 ± 0.09	-0.22 ± 0.10
[Ca/H]	+0.09 ± 0.11	-0.20 ± 0.12
[Sc/H]	+0.03 ± 0.06	...
[Ti/H]	+0.09 ± 0.11	-0.21 ± 0.07
[V/H]	+0.09 ± 0.07	...
[Cr/H]	-0.04 ± 0.06	...
[Mn/H]	-0.01 ± 0.08	...
[Co/H]	-0.02 ± 0.08	...
[Ni/H]	0.00 ± 0.06	-0.28 ± 0.08
log A(Li)	2.40 ± 0.10	2.52 ± 0.12
Spectral type	F9	F8
Age	7 ⁺² ₋₁ Gyr	5 ⁺³ ₋₂ Gyr
Distance	210 ± 20 pc	410 ± 70 pc

Notes: We determined $v \sin I_*$ from different subsets of spectra than the other parameters, as described in the text. The magnitudes are from the NOMAD catalogue (Zacharias et al. 2004). The spectral types are estimated from T_{eff} using Table B.1 in Gray (2008).

the values of log g_* and [Fe/H] in Table 4, but are interpolated at each MCMC step using the latest value of T_{eff} . The coefficient values corresponding to the best-fitting value of T_{eff} are given in Table 5. The transit lightcurve is parameterised by the epoch of mid-transit T_0 , the orbital period P , the planet-to-star area ratio $(R_p/R_*)^2$, the approximate duration of the transit from initial to final contact T_{14} , and the impact parameter $b = a \cos i_p / R_*$ (the distance, in fractional stellar radii, of the transit chord from the star’s centre in the case of a circular orbit), where a is the semimajor axis and i_p is the inclination of the orbital plane with respect to the sky plane.

The eccentric Keplerian radial-velocity orbit is parameterised by the stellar reflex velocity semi-amplitude K_1 , the systemic velocity γ , an instrumental offset between the HARPS and CORALIE spectrographs $\Delta\gamma_{\text{HARPS}}$, and $\sqrt{e} \cos \omega$ and $\sqrt{e} \sin \omega$ where e is orbital eccentricity and ω is the argument of periastron. We use $\sqrt{e} \cos \omega$ and $\sqrt{e} \sin \omega$ as they impose a uniform prior on e , whereas the jump parameters we used previously, $e \cos \omega$ and $e \sin \omega$, impose a linear prior that biases e toward higher values (Anderson et al. 2011b). The RM effect was modelled using the formulation of Giménez (2006) and, for similar reasons, is parameterised by $\sqrt{v \sin I} \cos \lambda$ and $\sqrt{v \sin I} \sin \lambda$.

The linear scale of the system depends on the orbital separation a which, through Kepler’s third law, depends on the stellar mass M_* . At each step in the Markov chain, the latest values of ρ_* , T_{eff} and [Fe/H] are input in to the empirical mass calibration of Enoch et al. (2010) (as based upon Torres et al. 2010 and as updated by Southworth 2011) to obtain M_* . The shapes of the transit lightcurves and the radial-velocity curve constrain stellar density ρ_* (Seager & Mallén-Ornelas 2003), which com-

bines with M_* to give the stellar radius R_* . The stellar effective temperature T_{eff} and metallicity [Fe/H] are proposal parameters constrained by Gaussian priors with mean values and variances derived directly from the stellar spectra (see Section 3).

As the planet-to-star area ratio is determined from the measured transit depth, the planet radius R_p follows from R_* . The planet mass M_p is calculated from the measured value of K_1 and the value of M_* ; the planetary density ρ_p and surface gravity log g_p then follow. We calculate the planetary equilibrium temperature T_{eq} , assuming zero albedo and efficient redistribution of heat from the planet’s presumed permanent day side to its night side. We also calculate the durations of transit ingress (T_{12}) and egress (T_{34}).

At each step in the MCMC procedure, model transit lightcurves and radial velocity curves are computed from the proposal parameter values, which are perturbed from the previous values by a small, random amount. The χ^2 statistic is used to judge the goodness of fit of these models to the data and the decision as to whether to accept a step is made via the Metropolis-Hastings rule (Collier Cameron et al. 2007): a step is accepted if χ^2 is lower than for the previous step and a step with higher χ^2 is accepted with a probability proportional to $\exp(-\Delta\chi^2/2)$. This gives the procedure some robustness against local minima and results in a thorough exploration of the parameter space around the best-fitting solution. To give proper weighting to each photometric data set, the uncertainties were scaled at the start of the MCMC so as to obtain a photometric reduced- χ^2 of unity. To obtain a spectroscopic reduced- χ^2 of unity we added ‘jitter’ terms in quadrature to the formal RV errors of WASP-20: 12 m s⁻¹ for the CORALIE RVs and 7 m s⁻¹ for the HARPS RVs; no jitter was required for WASP-28.

For both WASP-20b and WASP-28b we find, using the F -test approach of Lucy & Sweeney (1971), that the improvement in the fit to the RV data resulting from the use of an eccentric orbit model is small and is consistent with the underlying orbit being circular. We thus adopt circular orbits, which Anderson et al. (2012) suggest is the prudent choice for short-period, ~Jupiter-mass planets in the absence of evidence to the contrary. We find 2- σ upper limits on e of 0.11 and 0.14 for WASP-20b and WASP-28b, respectively.

Due to the low impact parameter of WASP-28b determinations of $v \sin I_*$ and λ are degenerate (Triaud et al. 2011; Albrecht et al. 2011; Anderson et al. 2011a). To ensure $v \sin I_*$ is consistent with our spectroscopic measurement, we imposed a Gaussian prior on it by means of a Bayesian penalty on χ^2 , with mean and variance as determined from the HARPS spectra (see Section 3). From an MCMC run with no prior we obtained $\lambda = -8 \pm 54^\circ$ and $v \sin I_* = 4.1^{+5.9}_{-0.9}$ km s⁻¹, with $v \sin I_*$ reaching values as high as 30 km s⁻¹, which is clearly inconsistent with the spectral measurement of $v \sin I_* = 3.1 \pm 0.6$ km s⁻¹. The degeneracy between $v \sin I_*$ and λ could be broken by line-profile tomography (Albrecht et al. 2007; Collier Cameron et al. 2010).

The median values and the 1- σ limits of our MCMC parameters’ posterior distributions are given in Table 6 along with those of the derived parameters. The best fits to the radial velocities and the photometry are plotted in Figures 1 and 2, with the RM effects highlighted in Figure 3. There is no evidence of additional bodies in the RV residuals (Figure 5).

We checked the effect of splitting the HARPS RVs for WASP-20 into two sets: those taken around the spectroscopic transit observation, spanning 2009 Oct 20–28, and the remainder. The fit to the RM effect was very similar to that when treating the HARPS RVs as a single dataset ($\lambda = 11.9 \pm 3.8^\circ$; $v \sin I_* = 4.75 \pm 0.51$ km s⁻¹).

Table 5. Limb-darkening coefficients

Planet	Instrument	Observation bands	Claret band	a_1	a_2	a_3	a_4
WASP-20	WASP / EulerCam	Broad (400–700 nm) / Gunn r	Cousins R	0.577	−0.042	0.484	−0.290
WASP-20	FTN / FTS	Sloan z'	Sloan z'	0.652	−0.345	0.635	−0.325
WASP-28	WASP / EulerCam	Broad (400–700 nm) / Gunn r	Cousins R	0.428	0.456	−0.175	−0.023
WASP-28	FTN	Sloan z'	Sloan z'	0.516	0.036	0.160	−0.135

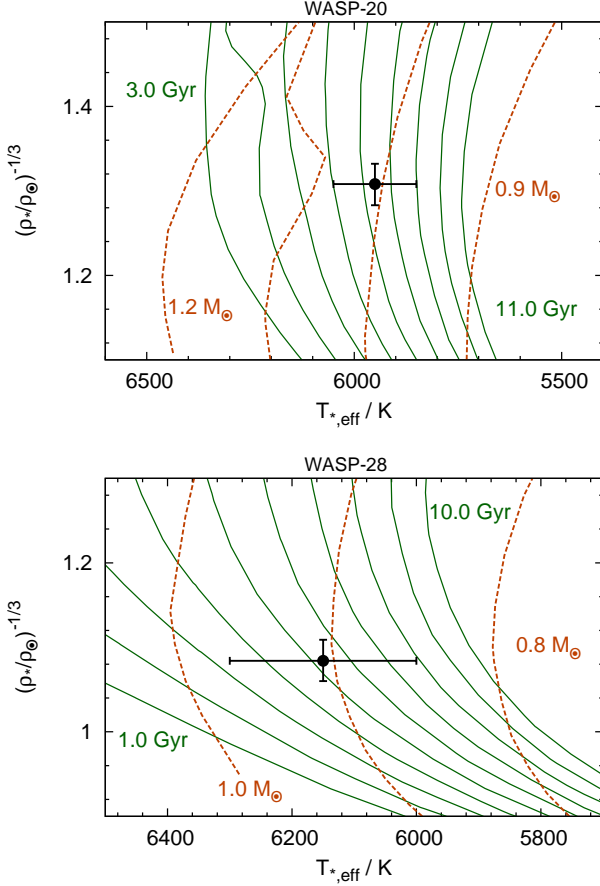


Fig. 6. Modified H–R diagrams. The isochrones, from Bressan et al. (2012), are in steps of integer Gyr with $Z = 0.0152$ for WASP-20 and $Z = 0.0078$ for WASP-28. The mass tracks, from Bertelli et al. (2008), are in steps of $0.1 M_{\odot}$ with $Z = 0.019$ for WASP-20 and $Z = 0.0097$ for WASP-28.

We interpolated the mass tracks of Bertelli et al. (2008) and the isochrones of Bressan et al. (2012) using ρ_* , T_{eff} and $[\text{Fe}/\text{H}]$ from the MCMC analysis (Figure 6). This suggests an age of 7^{+2}_{-1} Gyr for WASP-20 and 5^{+3}_{-2} Gyr for WASP-28. The mass tracks suggest a stellar mass of $1.02^{+0.07}_{-0.03} M_{\odot}$ for WASP-20 and $0.91 \pm 0.06 M_{\odot}$ for WASP-28. These are slightly lower than the masses derived from our MCMC analyses ($1.20 \pm 0.04 M_{\odot}$ for WASP-20 and $1.02 \pm 0.05 M_{\odot}$ for WASP-28), though they are consistent at the $2.3\text{-}\sigma$ (WASP-20) and $1.4\text{-}\sigma$ (WASP-28) levels.

5. Discussion

We present the discovery of WASP-20b, a Saturn-mass planet in a 4.9-day orbit around CD-24 102, and WASP-28b, a Jupiter-mass planet in a 3.4-day orbit around a $V=12$ star. Based on their masses, orbital distances, irradiation levels and metallicities, the radii of the planets ($1.46 R_{\text{Jup}}$ for WASP-20b and $1.21 R_{\text{Jup}}$ for

WASP-28b) are consistent with the predictions of the empirical relations of Enoch et al. (2012): $1.33 R_{\text{Jup}}$ for WASP-20b and $1.26 R_{\text{Jup}}$ for WASP-28b.

We find both planets to be in prograde orbits and, as the $v \sin I_*$ values are consistent with expectations for v for such stars, it is probable that $I_* \approx 90^\circ$ and so $\Psi \approx \lambda$. Assuming the spin axis of WASP-20 to be in the sky plane, the orbit of WASP-20b is aligned or near-aligned with the stellar spin ($\lambda = 8.1 \pm 3.6^\circ$). Although our determination for WASP-28b ($\lambda = 8 \pm 18^\circ$) is consistent with an aligned orbit, its low impact parameter results in a greater uncertainty.

Both host stars are near the posited boundary between efficient and inefficient aligners of $T_{\text{eff}} \approx 6250$ K (Winn et al. 2010; Schlaufman 2010). Both systems, with their low obliquity determinations, are consistent with the observation that systems with cool host stars and short expected tidal timescales are aligned (Albrecht et al. 2012 and references therein). With $M_{\text{p}}/M_* = 0.00025$ and $a/R_* = 9.3$, WASP-20b experiences relatively weak tidal forces. Its relative tidal dissipation timescale of $\tau_{\text{CE}} = 2.6 \times 10^{13}$ yr is the longest for the cool-host group barring HD 17156b (see section 5.3 of Albrecht et al. 2012).² With $M_{\text{p}}/M_* = 0.00084$ and $a/R_* = 9.5$, $\tau_{\text{CE}} = 2.5 \times 10^{12}$ yr for WASP-28b, placing it within the main grouping of aligned, cool-host systems. Assuming the planets did not arrive in their current orbits recently, the advanced age of both systems, 7^{+2}_{-1} Gyr for WASP-20 and 5^{+3}_{-2} Gyr for WASP-28, mean tidal dissipation would have occurred over a long timescale.

The planets may have arrived in their current orbits via planet-disc migration (Lin et al. 1996; Marzari & Nelson 2009) or via the scattering and circularisation route (Fabrycky & Tremaine 2007; Nagasawa et al. 2008; Matsumura et al. 2010; Naoz et al. 2011). Assuming the latter, the planets may have scattered into aligned orbits or they may have aligned with the spins of their host stars via tidal interaction, though how this could have occurred without the planets falling into their stars is currently a mystery (Barker & Ogilvie 2009).

Acknowledgements

WASP-South is hosted by the South African Astronomical Observatory and SuperWASP-North is hosted by the Isaac Newton Group on La Palma. We are grateful for their ongoing support and assistance. Funding for WASP comes from consortium universities and from the UK’s Science and Technology Facilities Council. M. Gillon is a FNRS Research Associate. A. H. M. J. Triaud is a Swiss National Science Foundation fellow under grant number PBGEP2-145594.

References

Albrecht, S., Reffert, S., Snellen, I., Quirrenbach, A., & Mitchell, D. S. 2007, *A&A*, 474, 565

² Note that these timescales are relative and that Albrecht et al. (2012) plot the timescales divided by 5×10^9 .

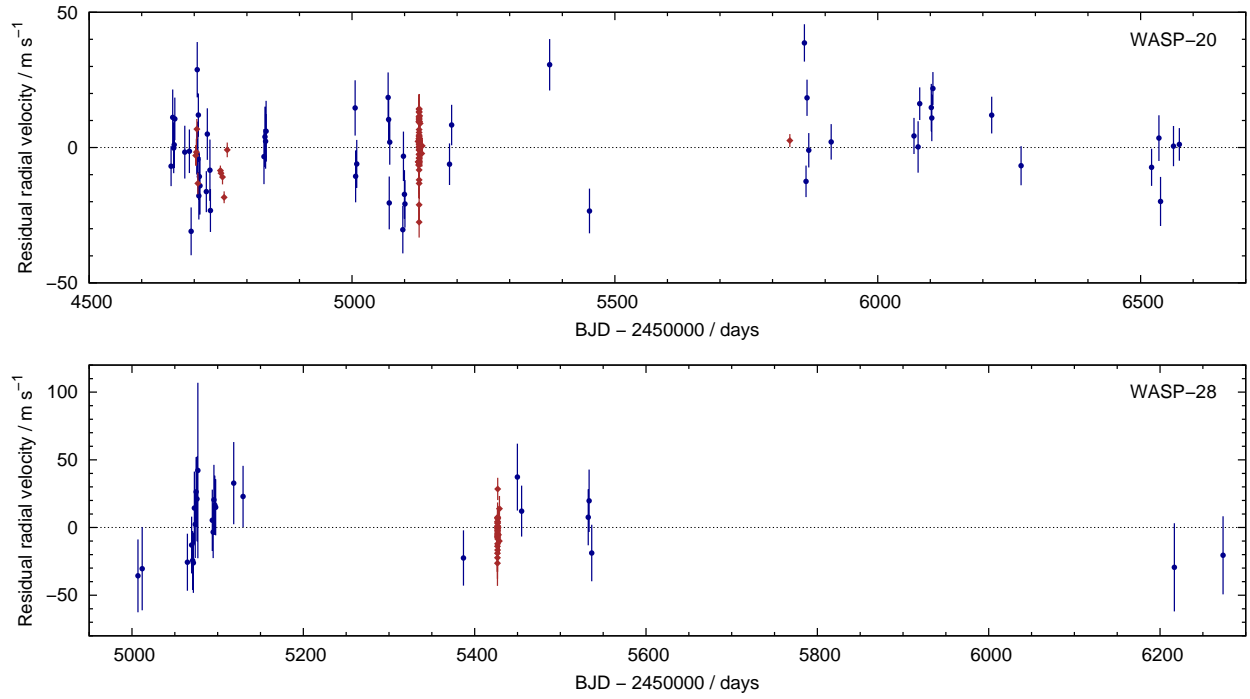


Fig. 5. The residuals about the best-fitting Keplerian orbits as a function of time (CORALIE in blue, HARPS in brown). There is no evidence of additional bodies.

- Albrecht, S., Winn, J. N., Johnson, J. A., et al. 2011, *ApJ*, 738, 50
 Albrecht, S., Winn, J. N., Johnson, J. A., et al. 2012, *ApJ*, 757, 18
 Anderson, D. R., Collier Cameron, A., Gillon, M., et al. 2012, *MNRAS*, 422, 1988
 Anderson, D. R., Collier Cameron, A., Gillon, M., et al. 2011a, *A&A*, 534, A16
 Anderson, D. R., Collier Cameron, A., Hellier, C., et al. 2011b, *ApJ*, 726, L19
 Bakos, G., Noyes, R. W., Kovács, G., et al. 2004, *PASP*, 116, 266
 Baranne, A., Queloz, D., Mayor, M., et al. 1996, *A&AS*, 119, 373
 Barker, A. J. & Ogilvie, G. I. 2009, *MNRAS*, 395, 2268
 Bate, M. R., Lodato, G., & Pringle, J. E. 2010, *MNRAS*, 401, 1505
 Bertelli, G., Girardi, L., Marigo, P., & Nasi, E. 2008, *A&A*, 484, 815
 Borucki, W. J., Koch, D., Basri, G., et al. 2010, *Science*, 327, 977
 Bressan, A., Marigo, P., Girardi, L., et al. 2012, *MNRAS*, 427, 127
 Brown, T. M., Baliber, N., Bianco, F. B., et al. 2013, *PASP*, 125, 1031
 Claret, A. 2000, *A&A*, 363, 1081
 Claret, A. 2004, *A&A*, 428, 1001
 Collier Cameron, A., Bruce, V. A., Miller, G. R. M., Triaud, A. H. M. J., & Queloz, D. 2010, *MNRAS*, 403, 151
 Collier Cameron, A., Pollacco, D., Street, R. A., et al. 2006, *MNRAS*, 373, 799
 Collier Cameron, A., Wilson, D. M., West, R. G., et al. 2007, *MNRAS*, 380, 1230
 Enoch, B., Collier Cameron, A., & Horne, K. 2012, *A&A*, 540, A99
 Enoch, B., Collier Cameron, A., Parley, N. R., & Hebb, L. 2010, *A&A*, 516, A33
 Fabrycky, D. & Tremaine, S. 2007, *ApJ*, 669, 1298
 Faedi, F., Barros, S. C. C., Pollacco, D., et al. 2011, *Detection and Dynamics of Transiting Exoplanets*, St. Michel l'Observatoire, France, Edited by F. Bouchy; R. Díaz; C. Moutou; EPJ Web of Conferences, Volume 11, id.01003, 11, 1003
 Giménez, A. 2006, *ApJ*, 650, 408
 Gray, D. F. 2008, *The Observation and Analysis of Stellar Photospheres* (Cambridge University Press)
 Greaves, J. S., Kennedy, G. M., Thureau, N., et al. 2014, *MNRAS*, 438, L31
 Hellier, C., Anderson, D. R., Collier Cameron, A., et al. 2011, *Detection and Dynamics of Transiting Exoplanets*, St. Michel l'Observatoire, France, Edited by F. Bouchy; R. Díaz; C. Moutou; EPJ Web of Conferences, Volume 11, id.01004, 11, 1004
 Lai, D., Foucart, F., & Lin, D. N. C. 2011, *MNRAS*, 412, 2790
 Lendl, M., Anderson, D. R., Collier-Cameron, A., et al. 2012, *A&A*, 544, A72
 Lin, D. N. C., Bodenheimer, P., & Richardson, D. C. 1996, *Nature*, 380, 606
 Lucy, L. B. & Sweeney, M. A. 1971, *AJ*, 76, 544
 Mandel, K. & Agol, E. 2002, *ApJ*, 580, L171
 Marzari, F. & Nelson, A. F. 2009, *ApJ*, 705, 1575
 Matsumura, S., Peale, S. J., & Rasio, F. A. 2010, *ApJ*, 725, 1995
 Maxted, P. F. L., Anderson, D. R., Collier Cameron, A., et al. 2011, *PASP*, 123, 547
 Mayor, M., Pepe, F., Queloz, D., et al. 2003, *The Messenger*, 114, 20
 McLaughlin, D. B. 1924, *ApJ*, 60, 22
 Nagasawa, M., Ida, S., & Bessho, T. 2008, *ApJ*, 678, 498
 Naoz, S., Farr, W. M., Lithwick, Y., Rasio, F. A., & Teyssandier, J. 2011, *Nature*, 473, 187
 Pepe, F., Mayor, M., Queloz, D., et al. 2005, *The Messenger*, 120, 22
 Pollacco, D., Skillen, I., Collier Cameron, A., et al. 2008, *MNRAS*, 385, 1576
 Pollacco, D. L., Skillen, I., Cameron, A. C., et al. 2006, *PASP*, 118, 1407
 Queloz, D., Henry, G. W., Sivan, J. P., et al. 2001, *A&A*, 379, 279
 Queloz, D., Mayor, M., Weber, L., et al. 2000, *A&A*, 354, 99
 Rogers, T. M., Lin, D. N. C., & Lau, H. H. B. 2012, *ApJ*, 758, L6
 Rossiter, R. A. 1924, *ApJ*, 60, 15
 Schlafman, K. C. 2010, *ApJ*, 719, 602
 Seager, S. & Mallén-Ornelas, G. 2003, *ApJ*, 585, 1038
 Southworth, J. 2011, *MNRAS*, 417, 2166
 Torres, G., Andersen, J., & Giménez, A. 2010, *A&A Rev.*, 18, 67
 Triaud, A. H. M. J. 2011, *A&A*, 534, L6
 Triaud, A. H. M. J., Collier Cameron, A., Queloz, D., et al. 2010, *A&A*, 524, A25+
 Triaud, A. H. M. J., Queloz, D., Hellier, C., et al. 2011, *A&A*, 531, A24
 Winn, J. N., Fabrycky, D., Albrecht, S., & Johnson, J. A. 2010, *ApJ*, 718, L145
 Zacharias, N., Monet, D. G., Levine, S. E., et al. 2004, in *Bulletin of the American Astronomical Society*, Vol. 36, American Astronomical Society Meeting Abstracts, 1418

Table 6. System parameters from the MCMC analyses

Parameter	Symbol	WASP-20	WASP-28	Unit
Orbital period	P	4.8996285 ± 0.0000034	3.4088300 ± 0.000006	d
Epoch of mid-transit	T_c	$2\,455\,715.65562 \pm 0.00028$	$2\,455\,290.40519 \pm 0.00031$	BJD (UTC)
Transit duration	T_{14}	0.1416 ± 0.0013	0.1349 ± 0.0010	d
Transit ingress/egress duration	$T_{12} = T_{34}$	0.0263 ± 0.0016	0.01441 ± 0.00070	d
Scaled orbital major semi-axis	a/R_*	9.29 ± 0.23	8.79 ± 0.19	
Planet-to-star area ratio	$\Delta F = R_p^2/R_*^2$	0.01161 ± 0.00022	0.01300 ± 0.00027	
Impact parameter	b	0.718 ± 0.018	0.21 ± 0.10	
Orbital inclination	i_p	85.57 ± 0.22	88.61 ± 0.67	$^\circ$
Stellar reflex velocity semi-amplitude	K_1	33.0 ± 1.7	120.5 ± 4.2	m s^{-1}
Systemic velocity	γ	$1\,316.222 \pm 0.080$	$24\,216.41 \pm 0.43$	m s^{-1}
Offset between HARPS & CORALIE	$\Delta\gamma_{\text{HARPS}}$	16.10 ± 0.74	6.0 ± 1.2	m s^{-1}
Eccentricity	e	0 (adopted; <0.11 at 2σ)	0 (adopted; <0.14 at 2σ)	
Sky-projected spin-orbit angle	λ	8.1 ± 3.6	8 ± 18	$^\circ$
Sky-projected stellar rotation velocity	$v \sin I_*$	4.71 ± 0.50	3.25 ± 0.34	km s^{-1}
Stellar mass	M_*	1.202 ± 0.040	1.021 ± 0.050	M_\odot
Stellar radius	R_*	1.392 ± 0.044	1.094 ± 0.031	R_\odot
Stellar surface gravity	$\log g_*$	4.232 ± 0.020	4.370 ± 0.018	(cgs)
Stellar density	ρ_*	0.447 ± 0.033	0.784 ± 0.058	ρ_\odot
Stellar effective temperature	T_{eff}	5950 ± 100	6150 ± 140	K
Stellar metallicity	[Fe/H]	-0.009 ± 0.061	-0.290 ± 0.10	
Planetary mass	M_p	0.313 ± 0.018	0.907 ± 0.043	M_{Jup}
Planetary radius	R_p	1.458 ± 0.057	1.213 ± 0.042	R_{Jup}
Planetary surface gravity	$\log g_p$	2.527 ± 0.036	3.149 ± 0.028	(cgs)
Planetary density	ρ_p	$0.1006^{+0.0131}_{-0.0099}$	0.508 ± 0.047	ρ_{Jup}
Orbital major semi-axis	a	0.06003 ± 0.00067	0.04469 ± 0.00076	AU
Planetary equilibrium temperature	T_{eq}	1379 ± 32	1468 ± 37	K